Published in final edited form as:
Electrophoresis. 2014 August ; 35(16): NA. doi:10.1002/elps.201470140.

Fast and Versatile Fabrication of PMMA Microchip Electrophoretic Devices by Laser Engraving

Ellen Flávia Moreira Gabriel[1,2], **Wendell Karlos Tomazelli Coltro**[1], and **Carlos D. Garcia**[2,*]

[1]Instituto de Química, Universidade Federal de Goiás, Goiânia, GO, 74001970, Brazil

[2]Department of Chemistry, The University of Texas at San Antonio, San Antonio, TX, 78249, USA

Abstract

This paper describes the effects of different modes and engraving parameters on the dimensions of microfluidic structures produced in PMMA using laser engraving. The engraving modes included raster and vector while the explored engraving parameters included power, speed, frequency, resolution, line-width and number of passes. Under the optimum conditions, the technique was applied to produce channels suitable for CE separations. Taking advantage of the possibility to cut-through the substrates, the laser was also used to define solution reservoirs (buffer, sample, and waste) and a PDMS-based decoupler. The final device was used to perform the analysis of a model mixture of phenolic compounds within 200 s with baseline resolution.

Keywords

CO_2-laser; engraving; capillary electrophoresis; microchips; amperometry

1. Introduction

The latest developments in miniaturization [1] have demonstrated the enormous potential of microfluidic devices for agricultural [2, 3], chemical, biomedical, and forensic applications [4, 5]. Among those devices designed for custom analytical and bioanalytical applications, microchip electrophoresis (ME) devices are some of the most important ones [6–8]. A variety of strategies have been employed in the production of devices for ME ranging from standard photolithography [9] to rapid prototyping [10–12] and assembly [13]. Although photolithographic techniques have been traditionally used to produce high-end devices using silica-based substrates, the process can be time-consuming and render chips that are (often) too expensive for most research laboratories. On the other extreme, techniques using paper and polyester-toner have been used to manufacture chips in less than 10 min with a cost lower than $ 0.10 per device, but the chemistry and topography of the materials often hinder the applicability of the technology [10, 14, 15]. Besides these examples, a range of polymers have emerged as alternative materials to fabricate ME devices [16–19]. In most cases, these plastics offer an adequate balance between fabrication procedures, cost, and analytical

*Corresponding author: Carlos D. Garcia, One UTSA Circle, San Antonio, TX, 78249, Phone: (210) 458-5774, Fax: (210) 458-5774, carlos.garcia@utsa.edu.

Authors have declared no conflicts of interest

performance. Polymeric materials can be divided into two main groups: elastomers (including for example, PDMS [20] and polyurethane [21]) and thermoplastics (comprising polycarbonate and PMMA). Due to its high mechanic and chemical stability, optical transparency, and excellent dielectric properties [22], PMMA has become one of the most popular substrates for ME systems. These properties have also allowed for the development of different fabrication methods including hot embossing [23], injection molding [24], and laser engraving [25, 26]. The latter is one of the most widely-used, non-contact type machining process in industry and can be applied across a wide range of materials [27].

Laser engraving of PMMA is typically accomplished using a CO_2 laser beam to break bonds in the polymer surface and remove the decomposed material from the ablated regions by the combination of photochemical and photo-thermal processes (melting, vaporization, and decomposition) [22]. Although traditionally limited by the resolution of the engraver, the process has been explored to fabricate microfluidic components for different applications including injectors [28], channels [29, 30], pumps [31], mixers [32], cytometers [33], valves [34], reactors [35], and devices for PCR amplification [36].

A number of commercial laser engravers and laser cutters are currently available. Among other sources available in the US market, Epilog (http://www.epiloglaser.com/), Gravograph (http://www.gravograph.us/), Mactron (http://www.co2-lasers.com/), Trotec (http://www.troteclaser.com), Universal (http://www.ulsinc.com/), and Xenetech (http://www.xenetech.com/) can be mentioned. As most of these systems are tailored toward specific applications linked to the graphic art industry (*and not towards making ME devices*), their size, speed, power, resolution, and cost varies widely. For the experiments described in this communication, we prioritized the minimum size of the laser spot, which defines the resolution of the instrument. In this context, this report describes the characterization of the variables affecting the engraving process (speed, power, frequency, resolution, and programmed line width) when applied to define microfluidic structures in PMMA substrates. Aiming to provide general guidelines to apply this technology in the fabrication of other devices, the engraving conditions were selected to produce either the smallest possible channels (vector mode) or the best defined structures (raster mode). In order to demonstrate the utility of the proposed fabrication method, devices were fabricated using the optimum conditions and used to perform the analysis of a mixture of phenolic compounds (dopamine, 2-aminophenol and catechol) by microchip-CE with amperometric detection.

2. Materials and Methods

2.1 Reagents and Solutions

Dopamine and 2-aminophenol were purchased from Alfa Aesar (Ward Hill, MA, USA). Sodium phosphate monobasic was received from Fisher Scientific (Waltham, MA, USA) and catechol was obtained from Acros (Geel, Belgium). All chemicals were used as received. The background electrolyte (10 mM phosphate buffer) was prepared weekly by dissolving the desired amount of solid NaH_2PO_4. The pH of the solutions was adjusted, when necessary, using either 1 $mol \cdot L^{-1}$ NaOH or 1 $mol \cdot L^{-1}$ HCl (Fisher Scientific) and measured using a glass electrode and a digital pHmeter (Orion 420A+, Thermo; Waltham,

MA). Stock solutions of dopamine, 2-aminophenol and catechol (10 mM each) were prepared by dissolving the desired amount of each compound in ultrapure water (≥ 18 MΩ·cm, NANOpure Diamond, Barnstead; Dubuque, Iowa). Working solutions were prepared by diluting the stock solutions in 10 mM phosphate buffer. Standard-grade PMMA plates (150 × 70 × 1.5 mm) were purchased from Gravograph (Duluth, GA, USA) and used to produce the microdevices herein described. Sylgard 184 silicone elastomer and curing agent were obtained from Dow Corning. Sugar, used for the formation of the PDMS sponge (decoupler), was food-grade and acquired in a local grocery store.

2.2 Instrumentation

A commercial laser engraver (Mini 24, 30W, Epilog Laser Systems, Golden, CO, USA) was used for all experiments described in this manuscript. This instrument was selected because (at the time of purchase) it was the most affordable one offering a resolution of 1200 dpi. The instrument features a CO_2 laser with a wavelength of 10.6 μm that perpendicularly hits the surface and is focused with the aid of lenses and a mechanical plunger (a manual focus option is also available). Translation of the beam across the platform (with a maximum linear speed of 1650 $mm \cdot s^{-1}$) is accomplished by a series of mirrors and motorized belts. The position of the beam is controlled by a software interface, which also allows setting the marking path, the scanning direction, and the conditions selected for the engraving process. The instrument has two engraving modes: raster and vector. The raster mode is used for marking materials and can only reach 1200 dpi when the line width is defined to be ≥127 μm. The vector mode, normally used to cut through substrates, can be programed to define lines (theoretically) as small as 25 μm (0.001 in). This resolution is about 1/10 of the spot size produced by a system manufactured by Symrad [37] and about 1/6 of the spot size produced by a system manufactured by Gravograph (600 dpi) [28]. In order to avoid exposure to monomers released to the working environment after the decomposition of the substrate, the vent of the engraver was connected to an air filter (model AD350, BOFA; Staunton, IL), equipped with a HEPA / activated aluminum potassium permanganate and an activated carbon panel. In order to minimize the deposition of debris on the surface of the PMMA substrates, the engraving head was also used to impinge a stream of N_2 (house line) on the engraving spot. These strategies also minimize the possibility of ignition of the vaporized material inside the engraver.

To evaluate the depth and width of the channels produced under each selected condition, a scanning electron microscope (SEM, JEOL/EO, JSM-6510; Peabody, MA, USA) was used. The obtained images were then analyzed using the manufacture's software. Complementary 3D images were obtained using an opto-digital microscope (Olympus DSX-500, Center Valley, PA) and analyzed using the manufacturer's software package.

Fabrication of PMMA devices—Besides being amenable to laser-engraving, PMMA was selected as the substrate because it is optically transparent, resistant to fouling, has adequate electro-osmotic properties, and can be chemically modified by a variety of reactions [38].

In order to rationally select the most appropriate conditions to produce channels on the PMMA surface, a multivariate approach was first attempted. However, none of the selected approaches was able to accurately describe (and predict) the effect of the experimental variables on the dimensions (depth and width) of the channels. Therefore, the following experiments describe results performed using a classic univariate approach, where each parameter was individually varied, while keeping the others constant. Based on preliminary experiments, the selected variables were: power, lateral speed, frequency, resolution, and programmed line width. In all cases, the selected pattern was designed using graphical software (CorelDraw Graphics Suite X6) and transferred to the engraver via a network-based printing protocol. In general, the time required for the fabrication step using the laser engraver depends on the material, the mode, the conditions selected, and the intricacy of the design. For example, engraving simple channels on the PMMA surface using the vector mode takes only a few seconds (to produce the microchip used for the experiments herein described required less than 5 s), which was comparable to the time required for other printing jobs sent from the same computer.

PMMA devices were produced using a previously designed layout [39]. These microchips consist of four reservoirs (3.0 mm wide), a double-T injector (split = 200 μm), a separation channel (4.8 cm effective length) and a series of channels to connect the reservoirs. An additional reservoir, placed 200 μm away from the waste reservoir, and filled with a PDMS “sponge” [40] was used as a decoupler. The decoupler, similar in design to the one reported by Lunte et al [41], was selected to minimize the formation of bubbles in the separation channel and decrease the noise of the detection step [42–44].

Briefly, the fabrication sequence began by laser-cutting the reservoir for the decoupler (*vide infra*, Figure 5A) in a flat layer of PMMA and casting a mixture of PDMS, curing agent (ratio of 10:1 by weight), and powdered sugar. Next, the PMMA layer was placed in the oven and kept at 80 °C for 20 min to cure the PDMS. Then, the substrate was immersed in deionized water and placed in the ultrasonic bath to dissolve the sugar and form the PDMS sponge. Next, the PMMA layer was placed again in the engraver to cut the solution reservoirs and engrave the channels. Once engraved, the PMMA substrate was rinsed with DI water (to remove debris deposited on the surface) and bonded to a blank piece of PMMA using a combination of pressure (the device clamped between two glass plates) and temperature (120 °C) for 10 min.

Electrophoresis and electrochemical detection—Injection and separation processes were performed with a 3-channel homemade high-voltage power supply with maximum voltage output of ± 4.0 kV [45] and standard Pt wires. Injection of the sample was performed using the floating method [46] by applying 800 V (duration of 10 s) between the sample and sample waste reservoirs, while keeping all other reservoirs floating. Then, the selected separation potential was applied between the buffer and the decoupler reservoirs, while floating the other reservoirs. All solution reservoirs were filled with the same volume (25 μL), and the electrophoresis experiments were performed at room temperature. End-channel amperometric detection [39] was selected to monitor the separation process. For all experiments, an electrochemical analyzer CHI 810B (CH Instruments, Inc, Austin, TX, USA) was used. A 25 μm gold wire was used as the working electrode and aligned at the

end of the separation channel perpendicular to the electrode channel. A platinum wire, placed in the buffer waste reservoir, was used as a pseudo-reference [47]. For all of the data reported here, the working electrode was set at a potential of + 700 mV (versus Pt), as defined by preliminary experiments (data not shown).

3. Results and Discussions

In general, the dimensions of the microchannel can be affected by two main sets of variables. The first group includes the thermophysical properties of the substrate. In this regard, and although a variety of plastics can be treated with CO_2 lasers [48], PMMA was selected because it presents high absorbance in the IR region ($\alpha \approx 0.92$), low heat capacity, and low conductance [49]. The second group of variables associated with the laser includes the incident power, lateral speed, frequency, and spot size. Therefore, the effect of each optical parameter of the engraver was investigated to define a set of conditions that would take advantage of the resolution of the engraver (1200 dpi) and produce structures with dimensions suitable for microfluidic devices.

3.1. Microfabrication of channels using vector mode

As previously stated, this engraving mode is typically used to cut-through the substrates and defines the smallest spot size. Therefore, the experiments herein described aim at taking advantage of the resolution of the system (1200 dpi) and define channels with dimensions adequate to fabricate ME devices.

Effect of speed and power—Figure 1A shows the effect of the engraving speed on the microchannel dimensions (depth and width). In this case, the speed (*X*-*Y* translation) was varied in a range between 10 and 100%, corresponding to 165 $mm \cdot s^{-1}$ and 1650 $cm \cdot s^{-1}$, respectively. As it can be observed, the speed at which the laser traveled across the surface has significant effects on both the width and the depth of the engraver channels. In general, the faster the speed, the smaller and narrower the channels. For example, displacing the beam at 10% of its speed results in channels that are 464 ± 2 μm deep and 122 ± 4 μm wide. However, if the speed is set at 100%, channels of 79 ± 1 μm×78 ± 1 μm can be obtained. This inversely proportional relation was somehow expected as the lateral speed controls the number of laser pulses applied per unit area [29]. As it can be seen in Figure 1B, the energy distribution of the laser beam on the surface [26, 49] resulted in Gaussian-shaped channels. Because higher speeds enabled the fabrication of channels with the smaller dimensions, a speed of 1650 $mm \cdot s^{-1}$ was selected as optimum and kept constant for the remaining experiments described in this manuscript.

The second variable influencing the dimensions of the channels was the laser power. Based on preliminary results, and considering that the instrument is furnished with a 30W laser, experiments were performed by varying the power from 10 to 50%. The results are summarized in Figure 2A. It is important to mention that while power values lower than 10% (< 3W) rendered poorly-defined channels; power values above the selected range (> 50% or > 15W) produced channels that were considered too big for microchip-CE applications. Within the selected range, an almost linear relationship was obtained between power and width/depth. Again, this trend can be attributed to the amount of energy delivered

to the surface of the PMMA, removing larger amounts of material and producing deeper and wider channels. Based on these results, a power of 10% (equivalent to 3W) was selected as optimum because it allows the fabrication of microdevices with the smallest channels. As an example of the topography obtained with the optimized conditions, Figure 2B shows a 3D image of the channels produced. Besides showing the shape of the channel, it is also evident in the figure that a small fraction of the material accumulates at the edge of the channel. This behavior has been attributed to the softening of polymer density caused by the irradiation, resulting in increases in volume and rise of the material [37, 49]

Effect of frequency, resolution and line width (dimensional accuracy)—Unlike the lateral speed and laser power, the frequency, resolution, and programmed line-width were found to have no statistical impact on the dimensions of the engraved microchannels using the vector mode. Results related to the effects of these variables on the dimensions of the channels have been included as Supplementary Information. It is also important to mention that although no significant differences were observed in the dimensions (depth or width) of the channels when frequencies in the 1000 to 5000 Hz range were selected, frequencies lower than 1000 Hz did not yield to the formation of complete microchannels in PMMA substrates. This was especially important when a combination of low frequencies and high speeds were programed, leading to the formation of a series of unconnected holes (also provided as supplementary information), where each laser pulse hit the surface. Based on these results and aiming to have the greatest flexibility in the experimental design, a frequency of 2500 Hz was selected for all experiments.

The second variable investigated was the resolution. In the case of the selected instrument, the resolution can be varied in the range of 150 to 1200 dpi (dots per inch). Although higher laser resolution equates to finer detail in the engraved features in raster mode, only small variations were obtained when the vector mode was used (selected to engrave the thinnest possible lines). In this case, it was observed that rather constant depths were obtained throughout the selected interval, showing only a small increase in the channel width at resolution values around 300 dpi. At 1200 dpi, the dimensions of the channels were found to be 70 ± 10 μm and 80 ± 10 μm in width and depth, respectively. It is important to mention that although these observations would not justify the purchase of a system with a resolution of 1200 dpi, the selected system could allow engraving other microfluidic elements (such as reactors or mixers using raster mode) at a lower scale (see Raster mode).

Next, the accuracy in which the engraver can produce channels with the dimensions programmed in the software (dimensional accuracy) was investigated. Again, and although it was expected that this variable would have critical effects on the dimensions of the features engraved using the raster mode, only small differences were obtained when line widths between 0.001 and 0.010 mm were programmed. In this case, channels with dimensions of 85 ± 7 μm (width) and 88 ± 5 μm (depth) were obtained. This behavior is the result of the selected engraving mode (vector), which is designed to focus the laser in a smaller area in order to cut through the material, ignoring the programmed line dimensions.

Number of laser passes and reproducibility—As mentioned earlier, due to the energy distribution of the laser beam engraved, channels adopt a Gaussian shape where the

dimensions can be mainly controlled by the laser speed and power. An additional approach that can be considered to control the dimensions of the engraved features is the number of passes of the laser beam. Klank and co-workers evaluated this effect for the first time using 1-mm thick PMMA substrates [26]. Keeping the laser speed and power constant, the authors found that the channel depth linearly increases with the number of passes while the channel width is only slightly affected. One year later, the same research group studied the influence of the cutting sequence, the number of cut passes, the laser beam velocity and the laser radiant flux over the microchannel dimension. The authors found that, at constant channel depth, the width can be varied as much as 27% by just altering the power and the number of laser passes [49]. Similar results were also found by Romoli et al. [37], who reported that in addition to the variations in the width of the channel, additional passes could favor the formation of large bulges over the cutting edges. In another report, it was found that the power multiplicity can cause an increase in both depth and width channel, while just the depth was changed when the multiple passes was employed [50]. For the experiments herein reported, the effect of the number of laser passes on the width and depth of the channels was investigated. Channels were cut with the CO_2 laser using a different number of passes (1 - 5) while keeping the speed (100%, 1650 mm·s^{-1}) and power (10%, 3W) constant. Figure 3 shows the dependence of width and depth as a function of the number of passes. As it can be observed, both the channel width and depth showed significant increases with the number of laser passes. According to these results by performing multiple engraving steps in the same position, the width and depth of the channel can be increased from 78 ± 1 μm to 115 ± 1 μm and from 84 ± 1 to 282 ± 1 μm, respectively. Although the possibility of engraving multiple passes certainly increases the versatility of the methodology, all microchips used in this manuscript were produced with a single pass.

Another important criterion to evaluate is the reproducibility of the proposed methodology. This parameter was evaluated in two ways. This first one was by comparing the dimensions of a series of channels (at least 5), consecutively made under the same experimental conditions. As it can be observed in the results presented in Figures 1–3 (error bars within the data points), the relative standard deviation in width and depth was in all cases lower than 7%. However, greater variances (up to 15%) were observed when channels were fabricated in different batches, where at least one variable was adjusted between channels (see Supplementary Information). Although these variations can slightly affect the dimensions and roughness of the channels formed, we consider that the ease and cost of the proposed fabrication procedure greatly surpass these limitations. In addition, if channels with very specific dimensions are required, a calibration step could be implemented.

3.2. Microfabrication of structures using raster mode

In order to fabricate microfluidic structures (other than channels), the possibility of using the engraver in raster mode was also investigated. This approach is an alternative to the one recently proposed by Do Lago and co-workers [35] who fabricated and characterized a glucose sensor using a laser-engraved microchannel. Other procedures to fabricate structures (although more complex in our view) have been also proposed [32]. As a complement to the vector mode, the raster mode can engrave features with lateral dimensions larger than 110 μm. Although not described in this manuscript, preliminary experiments indicated that using

50% power and 50% speed yield structures with depths lower than 200 μm, matching those obtained using the vector mode. Subsequently, the effect of the resolution was investigated by engraving a series of cylindrical pillars in 300, 600, and 1200 dpi. The process involves the removal of the PMMA in an area of 1 cm_2 leaving the pillars untouched. These structures resemble previously reported designs used to perform sample pretreatment or on-chip separations [51, 52]. As it can be observed in Figure 4, the resolution has a significant impact in the fabrication outcomes, significantly affecting the shape, roughness, and depth of the engraved elements. At 300 dpi (Figure 4A), it was observed that the shape of the pillars was not clearly defined, that the height of the resulting features was only 26 ± 5 μm, and that the roughness of the surrounding surface was 4.2 μm. At 600 dpi (resolution of most commercial instruments, Figure 4B), the pillars (77 ± 9 μm) can be clearly identified and the roughness of the surface decreased to 3.0 μm. At 1200 dpi, however, a much better definition of the programmed features was achieved, reaching a height of 128 ± 4 μm and a roughness of the engraved surface of just 1.4 μm. The results highlight the importance of using the highest possible resolution in this mode, which can have significant effects of the roughness and therefore in the resulting flow profile.

3.3. Integrated decoupler

As an additional capability, the laser engraver can be used to cut through the substrate by adjusting the variables in vector mode. For the substrates selected for this project, selecting 20% speed and 80% power was enough to cut through and define the reservoirs in the PMMA layer. In order to demonstrate this possibility, an additional reservoir was engraved at the end of the separation channel and used as a decoupler. Figure 5A shows the position of the decoupler with respect to the working electrode used for amperometric detection. To avoid introducing a significant amount of solution into the separation channel, this reservoir was filled with a PDMS sponge, fabricated from a mixture of PDMS and sugar. These PDMS sponges have been used by different research groups and applied to form conductive scaffolds containing carbon nanotubes [53] or to facilitate the absorption of gaseous CO_2 [54] or oil from water [40]. In this case, the PDMS sponge was selected as a decoupler because it is simple and can be easily produced, without incurring in significant additional expenses or metallic components (thin layers or wires). Most importantly, this approach was implemented to avoid the formation of bubbles on the electrode surface and reduce the noise level of the analysis caused by the interference of the electrophoretic current on the detection circuit. In accordance to previous reports [55–57], the decoupler was placed 200 μm away from the detection electrode, as a balance between noise reduction and diffusion. This distance was also considered optimal as it minimized the deformation of the substrate between the decoupler and the waste reservoir (also cut through) and results in consistent data after re-alignment of the PMMA layer during the fabrication process (that also requires engraving the channels).

In order to evaluate the performance of the proposed decoupler, the baseline noise was investigated as a function of the potential applied in the separation channel. For these experiments, the baseline noise (peakto- peak) was measured at the working electrode when the ground electrode (Pt) was placed either in the decoupler (D) or the waste reservoir (W). The results are summarized in Figure 5B. In general, significantly larger noise values were

obtained when the Pt electrode was placed in the waste reservoir, downstream from the detection circuit, reaching almost 2.5 nA when 1000V were applied. Although these values are relatively low, they indicate that the separation current is affecting the detection step. On the other side, when the Pt electrode was placed in the PDMS sponge (upstream from the detection electrode) an average of 91% reduction in the noise was obtained, reaching 0.4 nA at 1000V. The effect of other variables, including the shape of the decoupler or the composition of the sponge, was considered outside the scope of the present report.

3.4. Analytical performance of the PMMA device

As a proof-of-concept, the analytical performance of the PMMA device fabricated by CO_2 laser engraving was demonstrated by performing an analysis of a series of phenolic compounds (dopamine, 2-aminophenol, and catechol). The device consists of a decoupler and a series of microchannels fabricated using the conditions (speed, power, frequency, resolution and line-width) that produced the smallest dimensions. Conditions for the analysis (electrolyte concentration, pH, detection potential) were optimized based on previous reports from the group [58, 59]. As shown in Figure 6, cathodic migration (towards the waste reservoir) was observed for dopamine (pKa_1= 8.9, pKa_2= 9.6, pKa_3= 12.0) [60, 61] and 2-aminophenol (pKa_1= 4.78, pKa_2= 9.97) [62]. Catechol (pKa_1= 9.3, pKa_2= 13.3) [60, 63], was neutral in the selected background electrolyte. As it can be observed, all compounds were successfully separated within 200 s with baseline resolution. The migration times for dopamine, 2-aminophenol, and catechol were 60 s, 103 s and 150 s, respectively. The use of a decoupler ensured a good separation and prevented the formation of bubbles on the electrode surface.

The overall reproducibility of the process (from design to separation) was analyzed by comparing the separation of dopamine and catechol (100 μM each) obtained with three different devices. In such cases, variations lower than 10% were obtained for the respective migration times. This variation, which is likely to be the result of the slight variations reported for the engraving process (also within 10%), was considered acceptable for the scope of our work.

4. Conclusions

In summary, the effects of parameters of the CO_2 laser engraver systems in the production microchannel in PMMA substrate were extensively investigated. In addition, the use of a new decoupler fabricated using a mixture of PDMS/sugar was also investigated. The presented results show that the power and speed of the laser beam are the two most important parameters to control when the engraver is used in vector mode. Using a speed of 1.650 cm s^{-1} and power of 3 W, channels with dimensions in the 80 μm range (width and depth) can be systematically fabricated. Besides the power and speed, the number of passes of the laser beam showed a significant effect in the dimensions of the channels produced. Experiments performed using the raster mode allowed demonstrating the importance of selecting a system with the highest possible resolution. Although not incorporated in the final design, the possibility of engraving a series of well-defined pillars was demonstrated using 1200 dpi. The engraver was also used to integrate a PDMS-based decoupler,

preventing the formation of bubbles and minimizing the noise of the detection system. Overall, the proposed methodology presents itself as a viable option for fast fabrication of microchip-CE devices, minimizing the use of specialized facilities and speeding up the concept-to-device transition.

Supplementary Material

Refer to Web version on PubMed Central for supplementary material.

Acknowledgments

Financial support for this project has been provided in part by the University of Texas at San Antonio and the National Institutes of Health through the National Institute of General Medical Sciences (2SC3GM081085) and the Research Centers at Minority Institutions (G12MD007591). E.F.M.G. gratefully acknowledges the scholarship granted from Conselho Nacional de Desenvolvimento Científico e Tecnológico (CNPq) (Grant No. 246903/2012-0) and Instituto Nacional de Ciência e Tecnologia de Bioanalítica (Science without Borders Program). Authors would also like to thank Bill Chase (Olympus) for his help in the acquisition of the 3D images.

References

1. Ríos Á, Zougagh M, Avila M. Anal. Chim. Acta. 2012; 740:1–11. [PubMed: 22840644]
2. Neethirajan S, Kobayashi I, Nakajima M, Wu D, Nandagopal S, Lin F. Lab Chip. 2011; 11:1574–1586. [PubMed: 21431239]
3. Martín A, Vilela D, Escarpa A. Electrophoresis. 2012; 33:2212–2227. [PubMed: 22887146]
4. Horsman KM, Bienvenue JM, Blasier KR, Landers JP. J Forensic Sci. 2007; 52:784–799. [PubMed: 17553097]
5. Taudte RV, Beavis A, Wilson-Wilde L, Roux C, Doble P, Blanes L. Lab Chip. 2013; 13:4164–4172. [PubMed: 23959203]
6. West J, Becker M, Tombrink S, Manz A. Anal Chem. 2008; 80:4403–4419. [PubMed: 18498178]
7. Arora A, Simone G, Salieb-Beugelaar GB, Kim JT, Manz A. Anal Chem. 2010; 82:4830–4847. [PubMed: 20462185]
8. Garcia CD. Bioanalysis. 2012; 4:1717–1722. [PubMed: 22877217]
9. Segato TP, Coltro WKT, de Jesus Almeida AL, de Oliveira Piazetta MH, Gobbi AL, Mazo LH, Carrilho E. Electrophoresis. 2010; 31:2526–2533. [PubMed: 20665913]
10. Gabriel EFM, Duarte Junior GF, Garcia PdT, de Jesus DP, Coltro WKT. Electrophoresis. 2012; 33:2660–2667. [PubMed: 22965709]
11. Lucio do Lago C, Torres da Silva HD, Neves CA, Alves Brito-Neto JG, Fracassi da Silva JA. Anal. Chem. 2003; 75:3853–3858. [PubMed: 14572053]
12. Waldbaur A, Rapp H, Lange K, Rapp BE. Anal. Methods. 2011; 3:2681–2716.
13. Segato TP, Bhakta SA, Gordon MT, Carrilho E, Willis PA, Jiao H, Garcia CD. Anal. Methods. 2013; 5:1652–1657. [PubMed: 23585815]
14. Gabriel EFM, do Lago CL, Gobbi ÂL, Carrilho E, Coltro WKT. Electrophoresis. 2013; 34:2169–2176. [PubMed: 23712918]
15. Coltro WKT, de Jesus DP, da Silva JAF, do Lago CL, Carrilho E. Electrophoresis. 2010; 31:2487–2498. [PubMed: 20665911]
16. Castaño-Álvarez M, Fernández-Abedul MT, Costa-García A. Electrophoresis. 2005; 26:3160–3168. [PubMed: 16041703]
17. Mukhopadhyay R. Anal. Chem. 2007; 79:3234–3234. [PubMed: 17523223]
18. Focke M, Kosse D, Muller C, Reinecke H, Zengerle R, von Stetten F. Lab Chip. 2010; 10:1365–1386. [PubMed: 20369211]
19. Kuo JS, Chiu DT. Lab Chip. 2011; 11:2656–2665. [PubMed: 21727966]
20. Seethapathy S, Górecki T. Anal. Chim. Acta. 2012; 750:48–62. [PubMed: 23062428]

21. Domansky K, Leslie DC, McKinney J, Fraser JP, Sliz JD, Hamkins-Indik T, Hamilton GA, Bahinski A, Ingber DE. Lab Chip. 2013; 13:3956–3964. [PubMed: 23954953]
22. Chen Y, Zhang L, Chen G. Electrophoresis. 2008; 29:1801–1814. [PubMed: 18384069]
23. Yang S, Devoe DL. Methods in molecular biology (Clifton, N.J.). 2013:949.
24. Wang J, Pumera M, Chatrathi MP, Escarpa A, Konrad R, Griebel A, Dörner W, Löwe H. Electrophoresis. 2002; 23:596–601. [PubMed: 11870771]
25. Pugmire DL, Waddell EA, Haasch R, Tarlov MJ, Locascio LE. Anal. Chem. 2002; 74:871–878. [PubMed: 11866067]
26. Klank H, Kutter JP, Geschke O. Lab Chip. 2002; 2:242–246. [PubMed: 15100818]
27. Choudhury IA, Chong WC, Vahid G. Opt. Laser Eng. 2012; 50:1297–1305.
28. da Costa ET, Neves CA, Hotta GM, Vidal DTR, Barros MF, Ayon AA, Garcia CD, do Lago CL. Electrophoresis. 2012; 33:2650–2659. [PubMed: 22965708]
29. Sun Y, Kwok YC, Nguyen N-T. J Micromech Microeng. 2006; 16:1681–1688.
30. Nie Z, Fung YS. Electrophoresis. 2008; 29:1924–1931. [PubMed: 18393342]
31. Hsu Y-C, Chen T-Y. Biomed. Microdevices. 2007; 9:513–522. [PubMed: 17516175]
32. Riahi M. Microchem. J. 2012; 100:14–20.
33. Hong T-F, Ju W-J, Wu M-C, Tai C-H, Tsai C-H, Fu L-M. Microfluidics and Nanofluidics. 2010; 9:1125–1133.
34. Mohammed MI, Abraham E, Desmulliez MPY. J. Micromech. Microeng. 2013; 23:035034.
35. Cerdeira Ferreira LM, da Costa ET, do Lago CL, Angnes L. Biosens Bioelectron. 2013; 47:539–544. [PubMed: 23644059]
36. Lounsbury JA, Poe BL, Do M, Landers JP. J Micromech Microeng. 2012; 22:085006.
37. Romoli L, Tantussi G, Dini G. Opt. Laser Eng. 2011; 49:419–427.
38. Muck A, Svatoš A. Talanta. 2007; 74:333–341. [PubMed: 18371647]
39. García CD, Henry CS. Anal. Chem. 2003; 75:4778–4783. [PubMed: 14674454]
40. Choi S-J, Kwon T-H, Im H, Moon D-I, Baek DJ, Seol M-L, Duarte JP, Choi Y-K. ACS Appl. Mater. Interfaces. 2011; 3:4552–4556. [PubMed: 22077378]
41. Osbourn DM, Lunte CE. Anal. Chem. 2003; 75:2710–2714. [PubMed: 12948140]
42. Wang Y, Chen H, He Q, Soper SA. Electrophoresis. 2008; 29:1881–1888. [PubMed: 18393335]
43. Yu H, Xu X, Sun J, You T. Cent. Eur. J. Chem. 2012; 10:639–651.
44. Fischer DJ, Hulvey MK, Regel AR, Lunte SM. Electrophoresis. 2009; 30:3324–3333. [PubMed: 19802847]
45. Garcia CD, Liu Y, Anderson P, Henry CS. Lab Chip. 2003; 3:324–328. [PubMed: 15007467]
46. Roddy ES, Xu H, Ewing AG. Electrophoresis. 2004; 25:229–242. [PubMed: 14743476]
47. Schwarz MA, Galliker B, Fluri K, Kappes T, C. Hauser P. Analyst. 2001; 126:147–151. [PubMed: 11235094]
48. Klein, R. Laser Welding of Plastics. Wiley-VCH Verlag GmbH & Co. KGaA; 2011. p. 3-69.
49. Snakenborg D, Klank H, Kutter JP. J Micromech Microeng. 2004; 14:182–189.
50. Cheng J-Y, Wei C-W, Hsu K-H, Young T-H. Sensor Actuat B-Chem. 2004; 99:186–196.
51. Sainiemi L, Nissila T, Kostiainen R, Franssila S, Ketola RA. Lab Chip. 2012; 12:325–332. [PubMed: 22120065]
52. Seo JH, Kim SK, Zellers ET, Kurabayashi K. Lab Chip. 2012; 12:717–724. [PubMed: 22228264]
53. Han JW, Kim B, Li J, Meyyappan M. Appl. Phys. Lett. 2013; 102:051903.
54. Yuen PK, Su H, Goral VN, Fink KA. Lab Chip. 2011; 11:1541–1544. [PubMed: 21359315]
55. Liu Y, Vickers JA, Henry CS. Anal. Chem. 2004; 76:1513–1517. [PubMed: 14987111]
56. Lacher NA, Lunte SM, Martin RS. Anal. Chem. 2004; 76:2482–2491. [PubMed: 15117187]
57. Johnson AS, Selimovic A, Martin RS. Electrophoresis. 2011; 32:3121–3128. [PubMed: 22038707]
58. Ding Y, Ayon A, Garcia CD. Anal. Chim. Acta. 2007; 584:244–251. [PubMed: 17386611]
59. Ding Y, Mora MF, Merrill GN, Garcia CD. Analyst. 2007; 132:997–1004. [PubMed: 17893803]
60. Charkoudian LK, Franz KJ. Inorg. Chem. 2006; 45:3657–3664. [PubMed: 16634598]

61. Fausto R, Ribeiro MJS, de Lima JJP. J. Mol. Struct. 1999; 484:181–196.
62. Lin C-E, Chen Y-T. J. Chromatogr A. 2000; 871:357–366. [PubMed: 10735316]
63. Jewett SL, Eggling S, Geller L. J. Inorg. Biochem. 1997; 66:165–173.

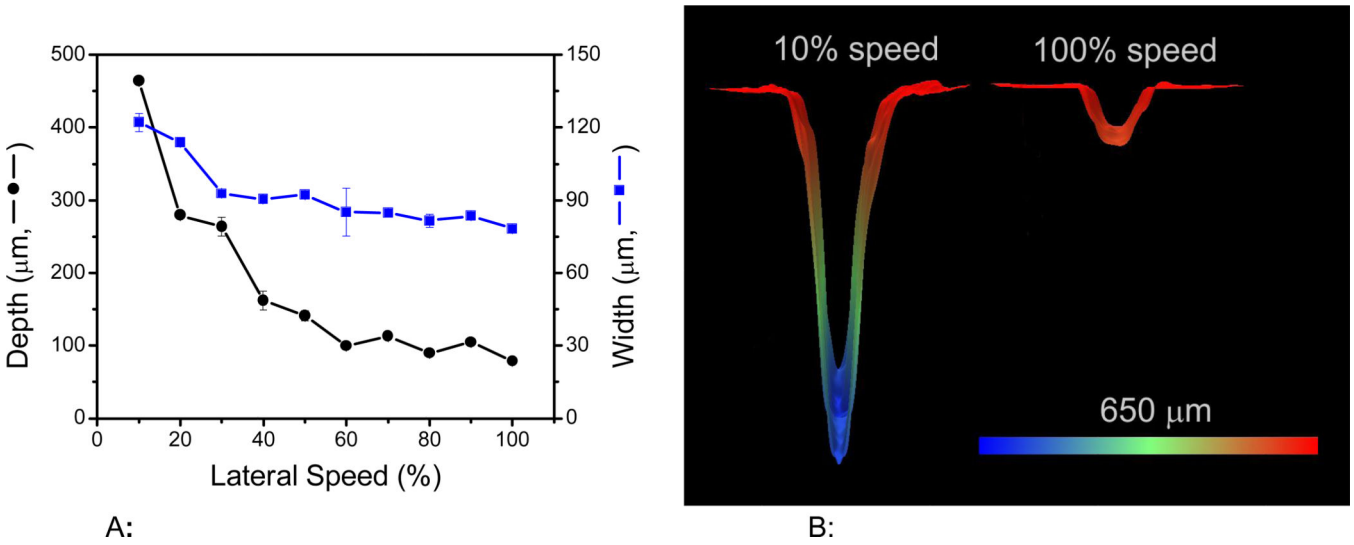

Figure 1.

Figure 1A: Effect of engraving speed on the microchannel dimensions. The relative values correspond to a maximum laser speed of 1650 mm·s^{-1}. Other conditions: power: 10%, frequency: 2500 Hz, resolution: 1200 dpi, and line-with: 10 μm.

Figure 1B: Representative 3D images of the channels obtained at either 100% or 10% lateral speed. Other conditions: power: 10%, frequency: 2500 Hz, resolution: 1200 dpi, and line-with: 10 μm.

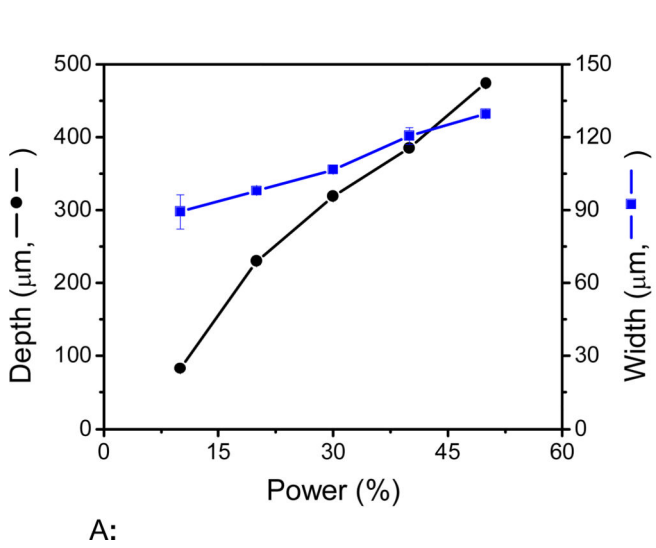

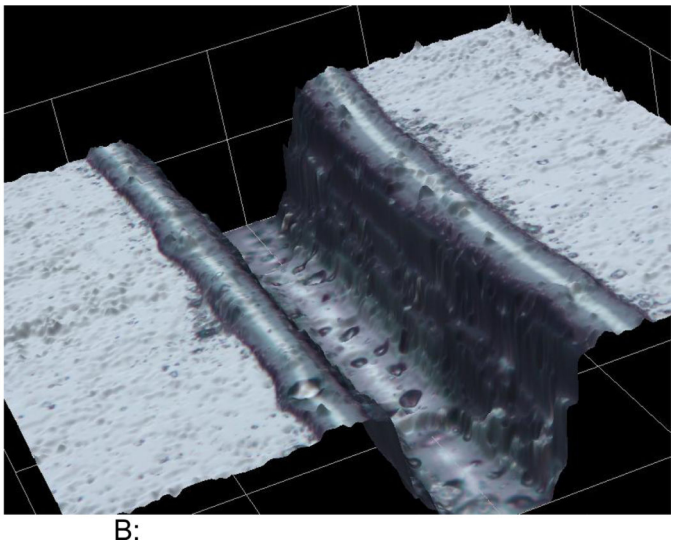

Figure 2.

Figure 2A: Effect of laser power on the microchannel dimensions. The relative values are based on maximum laser power of 30 W. Other conditions: lateral speed: 100%, frequency: 2500 Hz, resolution: 1200 dpi, and a programmed line-with: 10 μm.

Figure 2B: 3D image of a channel fabricated using 10% power (3W), 100% lateral speed, 2500 Hz, 1200 dpi resolution, and a programmed line-with of 10 μm.

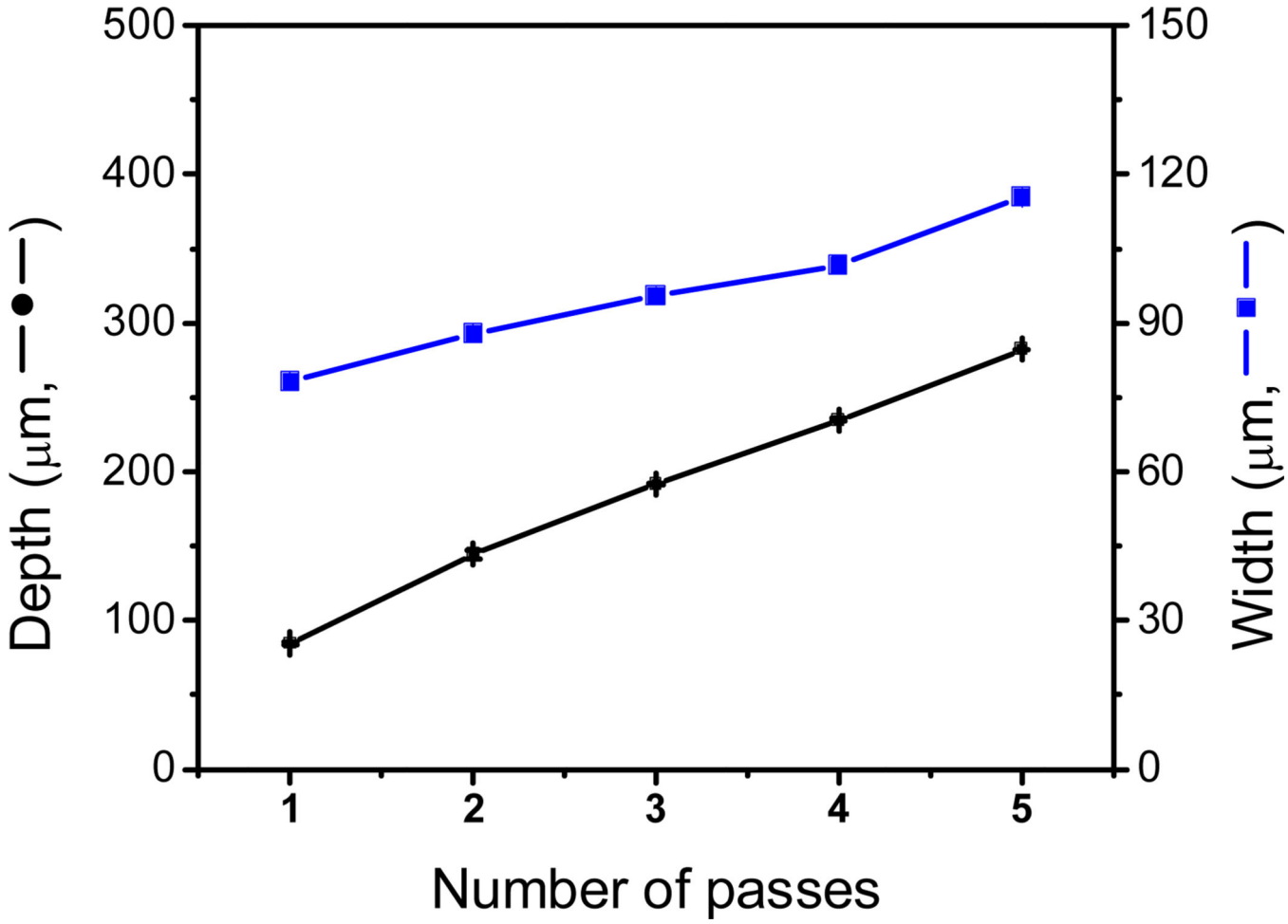

Figure 3.

Channel dimensions (depth and width) as a function of the number of laser passes. Channel fabricated using 10% power (3W), 100% lateral speed, 2500 Hz, 1200 dpi resolution, and a programmed line-with of 10 μm.

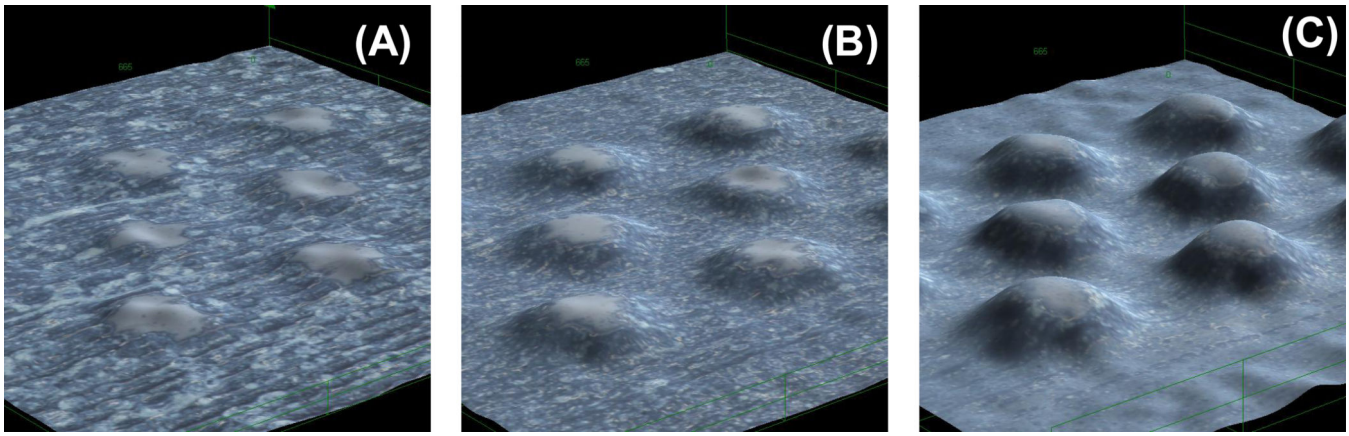

Figure 4.
Cylindrical pillars engraved using raster mode at (A) 300, (B) 600 and (C) 1200dpi.

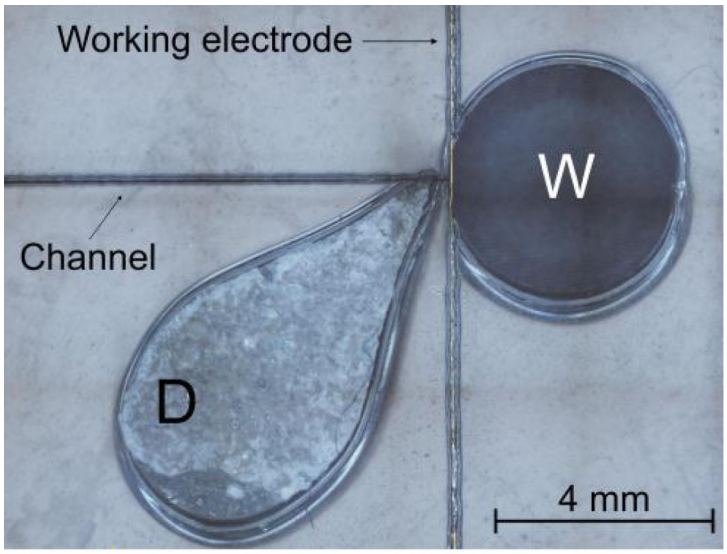

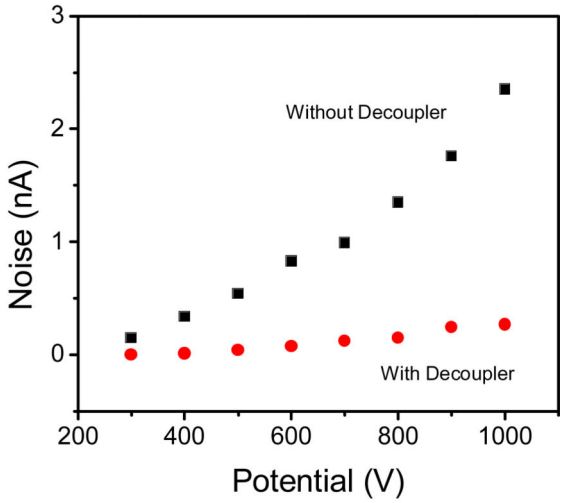

A: B:

Figure 5.

A: Position of the decoupler (PDMS sponge) with respect to the detection electrode and the waste reservoir.

Figure 5B: Peak-to-peak noise collected at the detection electrode as a function of the separation potential when the ground electrode was placed in either the waste (W) or the decoupler (D) reservoir.

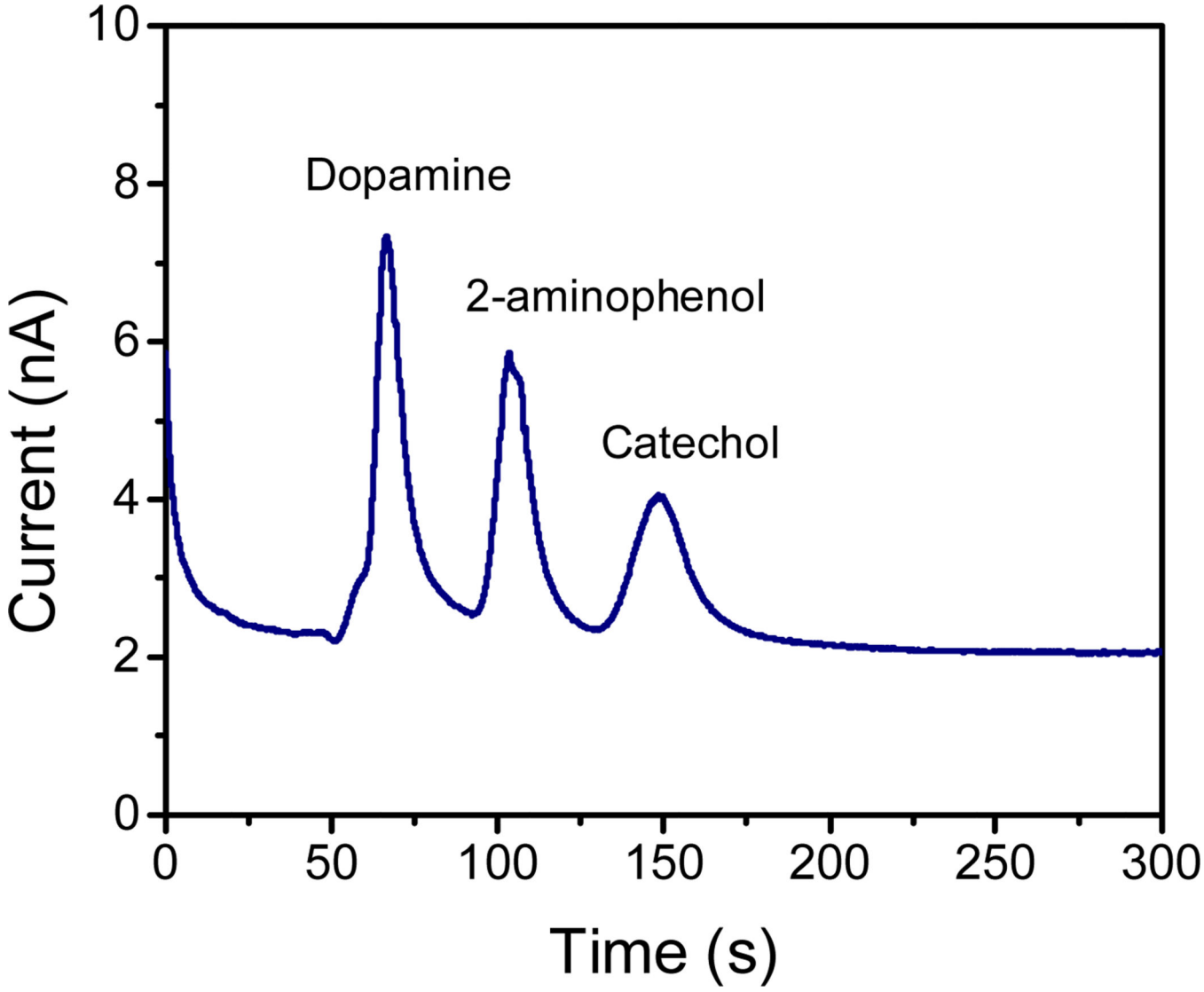

Figure 6.

Electrophoretic separation of dopamine, 2-aminophenol and catechol (100 μM each) on PMMA device produced with CO_2 laser. Running buffer: 10mM PBS (pH 7.5). Electrokinetic injection: 800 V during 10 s; Separation under an electric field of 160 $V \cdot cm^{-1}$. Amperometric detection at + 0.7 V (vs. Pt).